Measurement of the two-photon width of the η and η' mesons

N. A. Roe,* G. Bartha,† D. L. Burke, P. Garbincius,‡ C. A. Hawkins,§
M. J. Jonker,** and T. R. Steele††
Stanford Linear Accelerator Center, Stanford University, Stanford, California 94309

A. S. Johnson, J. S. Whitaker, and R. J. Wilson
Boston University, Boston, Massachusetts 02215

C. Hearty,* J. E. Rothberg, and K. K. Young
University of Washington, Seattle, Washington 98195

R. J. Hollebeek
University of Pennsylvania, Philadelphia, Pennsylvania 19104
(Received 10 April 1989)

Formation of the η and η' mesons in two-photon interactions has been observed with the ASP detector at the SLAC e^+e^- storage ring PEP ($\sqrt{s}=29$ GeV). In a data sample of 108 pb^{-1}, a total of 2287 η and 547 η' events have been detected in the $\gamma\gamma$ decay mode. The two-photon widths are determined to be $\Gamma_{\gamma\gamma}(\eta)=0.490\pm0.010\pm0.048$ keV and $\Gamma_{\gamma\gamma}(\eta')=4.96\pm0.23\pm0.72$ keV. The SU(3) pseudoscalar mixing angle deduced from these values is $\theta_p=-19.8°\pm2.2°$.

I. INTRODUCTION

Two-photon interactions at e^+e^- storage rings provide the opportunity to study the formation of neutral resonances with positive charge conjugation. The coupling of a neutral meson to two photons via its constituent quarks is proportional to the fourth power of the quark charges. A measurement of the two-photon width is therefore a probe of quark content and can be used both to test theoretical predictions for established mesons and to aid in the identification of exotic states which do not fit into the meson nonet structure.

In the case of the light pseudoscalar mesons $\eta(549)$ and $\eta'(958)$, there is an explicit prediction for the two-photon widths based on the triangle anomaly calculation of Adler, and Bell and Jackiw:[1]

$$\Gamma^{\eta}_{\gamma\gamma}=\frac{\alpha^2}{64\pi^3}\frac{M^3_{\eta}}{3}\left[\frac{1}{f_8}\cos\theta_P-\frac{\sqrt{8}}{f_1}\sin\theta_p\right]^2,$$
$$\Gamma^{\eta'}_{\gamma\gamma}=\frac{\alpha^2}{64\pi^3}\frac{M^3_{\eta'}}{3}\left[\frac{1}{f_8}\sin\theta_P+\frac{\sqrt{8}}{f_1}\cos\theta_P\right]^2, \quad (1)$$

where f_1 and f_8 are the singlet and octet decay constants of the SU(3) basis states η_1 and η_8, analagous to the pion decay constant $f_\pi=93$ MeV. The quark charges enter this prediction through the pseudoscalar mixing angle θ_p, which determines the quark content of the observed η and η' mass eigenstates in terms of the basis states of flavor SU(3) (Ref. 2):

$$|\eta\rangle=\cos\theta_P|\eta_8\rangle-\sin\theta_P|\eta_1\rangle,$$
$$|\eta'\rangle=\sin\theta_P|\eta_8\rangle+\cos\theta_P|\eta_1\rangle. \quad (2)$$

Thus, a measurement of the two-photon widths of the η and η' mesons provides a measure of θ_P.

II. EXPERIMENTAL SETUP

In this experiment, η and η' mesons (denoted P collectively, for pseudoscalar) were produced in untagged two-photon interactions, and were observed in the $\gamma\gamma$ decay mode:

$$e^+e^-\to e^+e^-\gamma^*\gamma^*\to e^+e^-P, \quad P\to\gamma\gamma. \quad (3)$$

In this expression, γ^* is used to denote a virtual photon; however, in an untagged two-photon reaction the photons are almost massless, or "quasireal." The data sample of 108 pb^{-1} was collected at the SLAC e^+e^- storage ring PEP ($\sqrt{s}=29$ GeV) with the ASP detector. The ASP detector has been described in detail elsewhere;[3] the features of the detector which are relevant for this analysis are briefly summarized below.

The ASP detector (Fig. 1) is a nonmagnetic, hermetic device which was designed for efficient detection of all-neutral final states over a large solid angle. The central calorimeter was constructed from 632 lead-glass bars of dimension $6\times6\times75$ cm^3, arranged in four quadrants of five layers each with the long axes of the bars perpendicular to the beam line. In the ASP coordinate system, the z axis is parallel to the beam line, the x axis points in toward the center of the PEP ring, and the y axis points vertically upward. The polar and azimuthal angles θ and ϕ are conventionally defined within this framework. The lead-glass calorimeter provides hermetic coverage over the full range in azimuth and for $20°<\theta_{\rm prj}<160°$, where projected theta is defined as the polar angle θ projected onto the vertical or horizontal plane normal to the lead-glass quadrant:

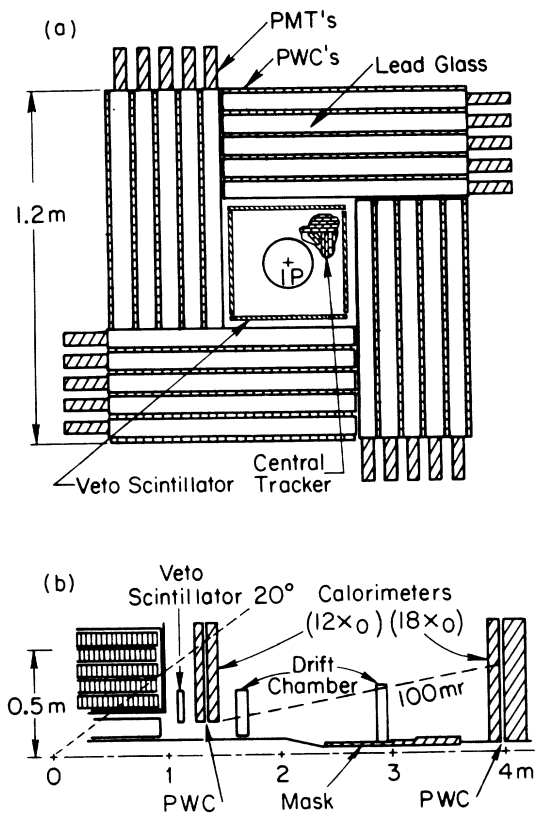

FIG. 1. (a) Cross section of the ASP central calorimeter and tracking system. Only a section of the central tracker is shown; it completely surrounds the IP. (b) Elevation view of one-quarter of the ASP detector. Only the horizontal lead-glass bars are shown.

$$\tan\theta_{\rm prj}=\frac{\sin\theta\times\max(|\cos\phi|,|\sin\phi|)}{\cos\theta}\ .$$

Projected theta is the natural unit to describe the acceptance in a square, rather than cylindrical, geometry.

Each lead-glass bar had a photomultiplier tube (PMT) glued to one end to detect Čerenkov light. The lead-glass calorimeter was 10 radiation lengths thick at normal incidence and had an energy resolution given by $\sigma_E=10\%\sqrt{E}$ (E in GeV). Interleaved with the lead glass were five layers of proportional wire chambers (PWC's) oriented orthogonally to the lead-glass bars. The central PWC's measured ϕ, while the lead-glass bars measured $\theta_{\rm prj}$; three-dimensional shower trajectories were reconstructed by combining clusters in the lead-glass bars with those in the central PWC's. Showers which were shared between two quadrants were reconstructed in two pieces, which were then combined by the pattern recognition routines. The errors on the reconstructed trajectories for tracks of 0.5 to 5 GeV were given by $\sigma_{\theta_{\rm prj}}=4.4°$ and $\sigma_\phi=3.2°$.

A central tracker inside the lead-glass calorimeter consisting of five layers of drift tubes provided charged-track identification. Charge division provided information along z, allowing the tracks to be unambiguously assigned to showers in the lead-glass calorimeter. Between the lead-glass calorimeter and the central tracker, veto scintillators were located to provide redundancy in charged-track identification. Above the lead-glass calorimeter a time-of-flight (TOF) system consisting of scintillator paddles suspended from the ceiling was used primarily to reject cosmic-ray events. Two forward calorimeter modules constructed from lead-scintillator sandwich were located on each side of the interaction point (IP), extending the coverage to within 21 mr of the beam line.

The physics triggers[4] were based on sums of the PMT signals from the lead-glass calorimeter, including the total energy, quadrant sums, and layers sums. In addition, diagnostic triggers recorded events from radiative Bhabha and low-angle Bhabha events, cosmic rays, and randomly selected beam crossings. The radiative Bhabha trigger was designed to record events with two low-angle, energetic showers in opposite forward calorimeters, in coincidence with a small amount of energy in the lead-glass calorimeter. The threshold on the lead glass was about 300 MeV, well below any of the other lead-glass trigger thresholds. This provided an independent sample which could be used to study the trigger performance.

The most important trigger for this analysis, the "two-photon" trigger, required 700 MeV of lead-glass energy deposited within ±20 ns of the beam crossing, with at least 150 MeV in the back four layers of one quadrant or of two opposite quadrants. In addition, no more than two of the inner veto scintillators were allowed to fire. These requirements reduced the contribution from beam-gas interactions. A further trigger requirement was made offline by imposing a software trigger cut on the raw lead-glass signal at 2400 counts, corresponding to approximately 700 MeV. This eliminated the turn-on region where the trigger efficiency was most sensitive to errors in the trigger simulation. The trigger efficiency will be discussed in more detail below.

III. EVENT SELECTION

The event-selection procedure required two neutral showers ("photons") within the acceptance of the lead-glass calorimeter, $20°\le\theta_{\rm prj}\le160°$. Both $\theta_{\rm prj}$ and ϕ were required to be well measured. In particular, this implied a significant energy deposit in at least two layers of the lead glass, as well as at least one layer hit in the central PWC. Each photon was required to originate from the IP: the distance of closest approach in z, $R=|Z|\sin\theta$ was required to be less than 30 cm, and the point of closest approach in the xy plane was required to be less than 10 cm if there were at least three layers hit in the PWC system. These cuts eliminated many beam-gas and cosmic-ray events.

The event was then vetoed if there was (1) more than 25 MeV of stray energy in the lead glass, (2) more than 150 (300) MeV of energy in the inner (outer) forward calorimeters, (3) time-of-flight information consistent with a cosmic-ray event, (4) a pattern of energy deposition in either the lead glass or the central PWC system

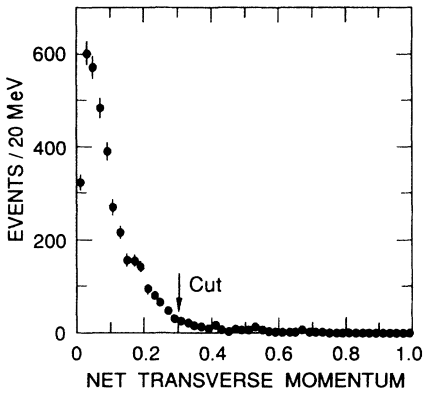

FIG. 2. Net-transverse-momentum distribution of final $\gamma\gamma$ sample. Events with net p_t greater than 300 MeV were rejected.

that was narrow and uniform, consistent with a minimum-ionizing track, or broad, consistent with two overlapping photons from the decay of a π^0; (5) more than 20 GeV of visible energy and an acollinearity of less than 10°. Cuts (1) and (2) eliminated beam-gas events and two-photon events with more than two particles in the final state. Cut (3) vetoed cosmic-ray events. The pattern cuts in (4) eliminated both cosmic-ray events and events containing π^0's. Cut (5) eliminated $e^+e^-\to\gamma\gamma$ events.

Finally, the acoplanarity angle (the difference in azimuthal angle) between the two photons was required to be greater than 135°, and the net p_t, defined as the vector sum of transverse momenta, was required to be less than 300 MeV/c. The net p_t distribution before these last two cuts were applied is shown in Fig. 2, for all events with invariant mass less than 2 GeV/c^2; the distribution is sharply peaked toward low p_t, as expected for two-photon interactions.

IV. ANALYSIS

The $\gamma\gamma$ invariant-mass spectrum of the final data sample is shown in Fig. 3. Clear peaks are evident at the η and η' masses. Some background due to two-photon production of the f_2 (1270), a tensor meson which has a large coupling to $\gamma\gamma$ and frequently decays to $\pi^0\pi^0$, is visible above the η'. These events from $f_2\to\pi^0\pi^0$ may pass the event-selection criteria if the two photons from the π^0 decay overlap or if one is undetected. (The f_2 peak is shifted down from the nominal mass due to the falling $\gamma\gamma$ flux and because low-energy photons from the π^0 decays may go undetected.)

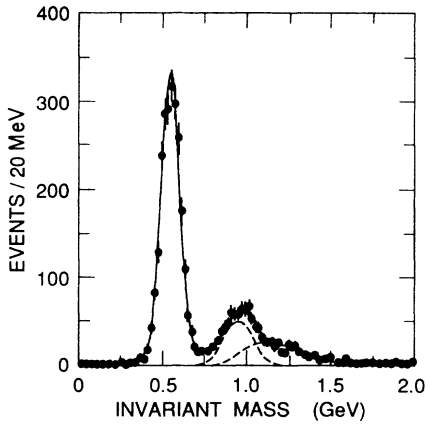

FIG. 3. Invariant-mass distribution of the final $\gamma\gamma$ sample. The solid line is the combined fit; the dashed line shows the η' and f_2 contributions.

The fit to the data (see Fig. 3) consists of the sum of two Gaussians with power-law tails to describe the η and η', and a Breit-Wigner fit with a total width of 176 MeV/c^2 convoluted with a Gaussian to describe the f_2. The form of the fitting function was determined using Monte Carlo data samples which had passed all event-selection criteria. (The Monte Carlo method is described below.) The mean and width of the η' and the f_2 were then fixed according to the results of the Monte Carlo simulation, because these parameters were highly correlated in the fit. The parameters describing the power-law tails of the η and η' were also fixed. The number of events in each peak was a free parameter, as were the mean and width of the η peak. The number of η events determined by the fit is 2380±49(stat)±25(sys), with a mean invariant mass of 545±1.3 MeV/c^2 and a width of 57±1.2 MeV/c^2, in good agreement with the results of the Monte Carlo simulation, and in reasonable agreement with the nominal η mass[5] of 548.8±0.6 MeV/c^2. The number of η' events is determined to be 568±26(stat) ±56(syst). Systematic errors for the number of η and the η' events were determined both by rebinning and by simultaneously varying the fixed parameters; the fit to the η' was particularly sensitive to the mass and Gaussian width of the f_2, resulting in a larger systematic error. The χ^2 probability of the fit was 47%.

The two-photon width is extracted from the fitted $\gamma\gamma$ invariant-mass spectrum according to

$$\Gamma^P_{\gamma\gamma}=\frac{N}{\tilde{\sigma}\mathcal{L}\epsilon B(P\to\gamma\gamma)}\ . \tag{4}$$

In this expression, P refers to either the η or η', and $\Gamma^P_{\gamma\gamma}$ is the two-photon width in keV. The quantities on the right-hand side of Eq. (4) are summarized in Table I, and their determination is discussed below.

The production cross section is given by the product $\tilde{\sigma}\Gamma^P_{\gamma\gamma}$; thus $\tilde{\sigma}$ has units of nb/keV. This quantity has been calculated using a QCD form factor:[6]

TABLE I. Summary of the quantities necessary for the calculation of the two-photon width of the η and η'.

	η	η'
Events from fit	2380±49±25	568±24±56
Background	93±51	21±4
Events−background	2287±49±57	547±24±56
$\tilde{\sigma}$ (nb/keV)	2.560±0.051	0.362±0.007
Efficiency	0.044±0.004	0.133±0.009
Luminosity (pb^{-1})	108.0±1.4	108.0±1.4
$\gamma\gamma$ branching ratio	0.389±0.004	0.0216±0.0016

$$F(q_1^2,q_2^2)=\frac{1}{(1+q_1^2/M^2)(1+q_2^2/M^2)}\ ,$$

$$M^2=0.68\ \text{GeV}^2\ . \quad (5)$$

This form factor differs from the ρ form factor only in the value of the mass, which for the ρ form factor is $m^2=M_\rho^2=0.59$ GeV^2. The total production cross section is significantly suppressed by the form factor, but for untagged events within the ASP detector acceptance the reduction in the cross section due to the form factor is slight, 1.5% for η events and 1.8% for η' events. As an estimate of the uncertainty in $\bar{\sigma}$ we take this difference between the accepted cross section with and without the form factor.

The integrated luminosity of the experiment, 108.0 ± 1.4 pb^{-1}, was determined using low-angle Bhabha scatters in the region 60 mr $<\theta<$ 90 mr (Ref. 7). The 1.3% error on the luminosity has three roughly equal contributions; in ascending order they are the statistical uncertainty, the systematic experimental uncertainty, and the theoretical uncertainty. The $\gamma\gamma$ branching ratios of the η and η' mesons are known from fixed-target experiments.[5]

The number of background-corrected events of each type is denoted by N; backgrounds which have been calculated include the fourth-order QED processes $e^+e^-\to e^+e^-\gamma\gamma$ and $e^+e^-\to e^+e^-e^+e^-$, where the electrons are misidentified as neutral, the two-photon processes $\gamma\gamma\to a_2(1320)\to\eta\pi^0$ and $\gamma\gamma\to\pi^0\pi^0$ in the continuum, as well as cosmic-ray and beam-gas backgrounds. The only significant background contributions in the η region are from continuum $\gamma\gamma\to\pi^0\pi^0$ production and from beam-gas interactions. The former has been estimated using the Monte Carlo simulation and recent experimental data[8] to be 37 ± 19 events. The latter was estimated both by selecting events produced away from the IP in z and by direct calculation.[9] The two methods were in good agreement, although both had large errors; the average result was 53 ± 47 events. In the η' region, the dominant background from the $f_2(1270)$ is determined by the fit to the data. The other backgrounds in the η' region, which are all small and contribute about equally, are $e^+e^-\to e^+e^-\gamma\gamma$, and two-photon production of $a_2\to\eta\pi^0$ and $\pi^0\pi^0$ in the continuum.

The efficiency ϵ is given by the product of the detector acceptance, the trigger efficiency, and the event-selection efficiency. These factors were determined by generating unweighted η and η' events according to the exact differential cross section, using a Monte Carlo program based on the work of Vermaseren.[10] An equivalent integrated luminosity of about seven times greater than that of the data was generated. The events were passed through a detector simulation routine based on the EGS electromagnetic-shower simulation program.[11] The detector acceptance, which is determined by requiring two photons in the region $20°<\theta_{\rm prj}<160°$ and no electron scattered above 21 mr, was $(25.9\pm0.9)\%$ for $\eta\to\gamma\gamma$ events and $(30.6\pm0.9)\%$ for $\eta'\to\gamma\gamma$ events, where the errors are systematic due to uncertainty in the detector geometry.

The trigger efficiency was determined using a detailed trigger simulation which included threshold effects, dead channels, and attenuation of Čerenkov light in the lead-glass bars. The software trigger cut was also imposed; in this region above approximately 700 MeV the trigger efficiency was high and fairly flat. The combined hardware and software trigger efficiency for events within the detector acceptance was $(40.9\pm2.4)\%$ for the η and $(94.7\pm1.1)\%$ for the η', where the errors are systematic and are discussed below.

The trigger efficiency was much lower for η events because the trigger threshold was above the η mass of 549 MeV; only those events in which the η was produced with a longitudinal boost satisfied the trigger. The effect of the trigger on η events can be seen in Fig. 4(a). The data points show the total energy distribution of η events from the final $\gamma\gamma$ data sample ($0.4<M_{\gamma\gamma}<0.7$ GeV), without the software trigger imposed. The solid histogram represents the Monte Carlo simulation for the same requirements. The dashed histogram is the Monte Carlo simulation without either the hardware or software triggers imposed. The loss in efficiency due to the hardware trigger is clearly evident; the good agreement between the data points and the solid histogram indicate that the trigger and simulation is quite accurate. A similar comparison, shown in Fig. 4(b), was made using a data sample of 2.2×10^5 untagged events from the

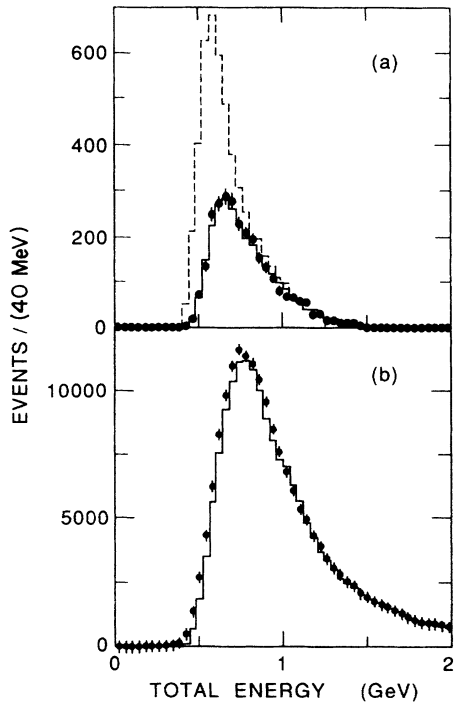

FIG. 4. (a) Total-energy distribution for $\eta\to\gamma\gamma$ events. The dashed curve is the Monte Carlo simulation with no trigger imposed; the histogram is the same with the trigger requirement. The points are η events from the final $\gamma\gamma$ data sample. (b) Total-energy distribution for untagged $e^+e^-\to(e^+e^-)e^+e^-$ events. This histogram is the Monte Carlo simulation with the trigger requirement imposed; the points are data.

fourth-order QED process $e^+e^- \to (e^+e^-)e^+e^-$. In this high-statistics study, the total energy distribution of the Monte Carlo simulation reproduced the data very well; the slight discrepancy at low energy was folded with the energy distribution of η and η' events to determine the systematic error on the trigger efficiency.

The efficiency of the event-selection criteria for events within the detector acceptance which also satisfied the trigger was $(41.8\pm2.4)\%$ and $(45.8\pm2.6)\%$ for η and η' events, respectively. Uncertainties in detector simulation were the dominant source of systematic error; they have been determined by detailed comparison of Monte Carlo simulation with data. This was performed by making an unbiased selection of radiative Bhabha events by requiring a radiative Bhabha trigger and an acceptable χ^2 for a kinematic fit to a three-body final state. This resulted in a very clean sample of events with a single photon in the lead-glass calorimeter. (Events with single electrons were also selected; with the exception of some hits in the central tracker and veto scintillator they are very much like photons.) Next, a Monte Carlo sample of single photons was generated using the kinematically fitted parameters of real events to determine the energy and angular distribution. The efficiency for a photon to pass a given cut was then determined for both the Monte Carlo and data samples, and the discrepancy between them was folded with the energy and angular distributions of the η and η' events to determine the systematic error.

V. RESULTS AND CONCLUSIONS

Using Eq. (4) and the results summarized in Table I yields the following results for the two-photon widths:

$$\Gamma_{\gamma\gamma}(\eta)=0.490\pm0.010\pm0.048 \text{ keV} ,$$

$$\Gamma_{\gamma\gamma}(\eta')=4.96\pm0.23\pm0.72 \text{ keV} ,$$

where the first error is statistical and the second is systematic. The dominant source of error for the η is the uncertainty in the trigger efficiency; for the η', the largest contribution to the error is due to uncertainty in the background from the f_2. These values are in good agreement with the two-photon world-average values, $\Gamma_{\gamma\gamma}(\eta)=0.534\pm0.031$ keV and $\Gamma_{\gamma\gamma}(\eta')=4.28\pm0.22$ keV (Ref. 12). However, the two-photon results for $\Gamma_{\gamma\gamma}(\eta)$ are in disagreement with an earlier measurement of this quantity using the Primakoff technique;[13] the source of this discrepancy is not understood.[14]

The pseudoscalar mixing angle calculated using Eq. (1) is $\theta_P=-19.8°\pm2.2°$. The singlet decay constant is determined to be $f_1=(1.02\pm0.14)f_\pi$. In this calculation we have not assumed nonet symmetry; the near equality of f_1 and f_π comes out naturally. To solve Eq. (1), we have used $f_8=1.25f_\pi$, based on a calculation which incorporates SU(3)-symmetry breaking at the one-loop level in chiral perturbation theory,[15] and have assigned a theoretical error of 5% on this calculation.[2]

This value of θ_P is also in agreement with the pseudoscalar mixing angle calculated using the Gell-Mann–Okubo mass formula, provided SU(3)-breaking effects are also incorporated in this calculation.[15] Thus a consistent picture of mixing in the pseudoscalar-meson nonet has emerged based on recent experimental evidence and theoretical calculations.

ACKNOWLEDGMENTS

We acknowledge useful discussions with F. Gilman and R. Kauffman, and constructive criticism of the manuscript by P. Extermann. We thank D. Chambers, R. Baggs, D. Forbush, L. Keller, T. Lyons, C. Matteuzzi, C. Noyer, K. Skarpass, and R. Stickley for considerable technical assistance with the construction and installation of the detector. We are also grateful to the PEP operations staff. This work was supported by Department of Energy Contracts Nos. DE-AC03-76SF00515, DE-AC02-863440284, and DE-AC02-76ER03071, and by National Science Foundation Grant No. PHY-8503215.

*Present address: Lawrence Berkeley Laboratory, Berkeley, CA 94720.

†Present address: University of Southern California, Los Angeles, CA 90007.

‡Present address: Fermi National Laboratory, Batavia, IL 60510.

§Present address: ESL, Sunnyvale, CA 94088.

**Present address: CERN, EP Division, Geneva CH-1211, Switzerland.

††Present address: Lightwave Electronics, Mountain View, CA 94043.

[1]S. Adler, Phys. Rev. **177**, 2426 (1969); J. S. Bell and L. Jackiw, Nuovo Cimento **60**, 47 (1969).

[2]For a summary of SU(3) formalism and a review of current experimental results on θ_P, see F. Gilman and R. Kauffman, Phys. Rev. D **36**, 2761 (1987).

[3]G. Bartha *et al.*, Nucl. Instrum. Methods **A275**, 118 (1989).

[4]R. J. Wilson, in *Proceedings of the Workshop on Triggering, Data Acquisition and Computing for High Energy/High Luminosity Hadron-Hadron Colliders,* edited by B. Cox, R. Fenner, and P. Hale (Fermilab, Batavia, IL 1986), p. 118.

[5]Particle Data Group, G. P. Yost *et al.*, Phys. Lett. B **204**, 1 (1988).

[6]S. Brodsky and P. Lepage, Phys. Rev. D **24**, 1808 (1981).

[7]C. A. Hawkins, Ph.D. thesis, Stanford University, SLAC Report No. 337, 1989.

[8]H. Marsiske, Ph.D. thesis, Hamburg University, 1988.

[9]For more details, see N. A. Roe, Ph.D. thesis, Stanford University, SLAC Report No. 338, 1989.

[10]J. Vermaseren, Nucl. Phys. **B229**, 347 (1983).

[11]R. L. Ford and W. R. Nelson, Report No. SLAC-PUB-0210, 1978 (unpublished).

[12]For a recent summary, see D. Williams *et al.*, Phys. Rev. D **38**, 1365 (1988).

[13]A. Browman *et al.*, Phys. Rev. Lett. **32**, 1067 (1974).

[14]For a discussion of this problem, see N. A. Roe (Ref. 5), p. 170.

[15]J. Donoghue, B. Holstein, and Y. Lin, Phys. Rev. Lett. **55**, 2766 (1985).